Numerical Investigation of Interrupted Microchannel Heat Sink with Multi-Step Rectangular Ribs in the Transverse Microchambers

Hossein Karbasian, Abas Ramiar*[ID] , Amirhosein Ghasemi

Mechanical Engineering Deparment, Babol Noshirvani University of Technology, Babol, Iran.

ARTICLE INFO

Article Type
Original Research

ABSTRACT

This study numerically explores the performance of multi-step rectangular ribs and their base surfaces in microchannel heat sinks using the finite volume method in ANSYS Fluent. To reduce computational cost, a symmetry-based approach was employed on a representative section of the microchannel.

Among the rib designs, double-step ribs demonstrated superior thermal performance, with a 14% increase in the thermal enhancement factor. Key metrics included a 27.3% rise in the Nusselt number and a 41% increase in friction factor. The initial friction increase stems from vortex formation by rib steps, though this effect diminishes at higher Reynolds numbers.

Further analysis revealed that expanding the top step surface area in double-step ribs yields notable benefits. When A_2 was set to 1.5A, the thermal enhancement factor rose by 25%, while the Nusselt number and friction factor increased by 42% and 51%, respectively.

These optimized rib structures show strong potential for industries demanding high-efficiency thermal management. Applications include electronics cooling—improving heat dissipation in processors and circuit boards; electric and hybrid vehicle systems—enhancing battery regulation and longevity; and high-performance computing and data centers—reducing cooling costs and improving reliability. The ribs also offer advantages in aerospace, avionics, and precision medical devices such as laser systems.

By integrating advanced rib geometries into microchannel heat sinks, engineers can significantly improve heat transfer and durability across a range of sectors.

Keywords: Heat Transfer, Microchannel Heat Sink, Multi-Step Rib, Numerical Simulation.

Corresponding author's email: aramiar@nit.ac.ir
Corresponding ORCID ID: 0000-0003-0777-2778

1-Introduction

In today's modern world, computers are crucial, from portable devices like smartphones and laptops to industrial applications such as PCs and data centers. With increasing dependency on computing power, especially with AI in various fields, computers have become more powerful, requiring more power, thus generating more heat. Managing this heat is crucial as temperature overload is the main cause of electronics failure. Thus, advanced and efficient heat transfer systems are more critical than ever. Among various methods, including air cooling, phase-change cooling, thermoelectric cooling, heat pipes, vapor chambers, and immersion cooling, liquid cooling stands out as the most efficient for high-performance applications. It leverages the higher heat capacity of liquids to absorb and dissipate heat more effectively than air cooling, making it an ideal option for powerful components like CPUs and GPUs. Liquid cooling systems operate quietly, scale well, and use micro heat sinks with microchannels to maximize heat transfer, making them ideal for ensuring optimal performance and longevity of electronic devices.

In recent years, many efforts were made to increase the efficiency of micro channel heat exchangers. Earlier works used air as working fluid. Dogan and Sivrioglu[1] investigated the mixed convection heat transfer from longitudinal fins within a horizontal channel, maintaining a uniform heat flux boundary condition at the bottom surface throughout the experiments. Air served as the working fluid, and a constant heat flux was applied. Their study presented experimental results for bottom-heated fin arrays, examining various fin spacings, fin heights, and modified Rayleigh numbers, while analyzing their effects on heat transfer. They found that the heat transfer performance improved significantly with optimized fin spacing and height, but also noted an increase in pressure drop. Soeyi and colleagues[2] conducted an experimental study using wavy microchannels with rectangular cross-sections. In their experiments, they used air as the working fluid to simulate real-world cooling scenarios. The results showed that the heat transfer performance improved by 211 percent compared to a simple channel, while the pressure drop observed an increase of 76 percent.

Kuppusamy et al.[3,4] conducted numerical investigations on the effects of geometrical parameters in trapezoidal and triangular grooves. They discovered that triangular grooves exhibited superior performance compared to trapezoidal grooves. This enhanced performance was attributed to the ability of triangular grooves to create larger vortices, which promote better flow mixing. They also noted that increasing the angle and depth of the grooves expands the groove zone, providing more space for these larger vortices to form, thereby enhancing the overall hydrothermal performance.

Xia et al.[5–9] conducted both numerical and experimental studies to investigate the effects of various re-entrant cavity shapes on the hydrothermal performance of microchannels, including aligned fan-shaped, offset fan-shaped, and triangular re-entrant cavities. Their research showed that microchannels with re-entrant cavities generally exhibited superior heat transfer performance compared to straight microchannels. The enhancement in heat transfer was attributed to the increased surface area and disruption of the thermal boundary layer caused by the cavities. Among the studied configurations, triangular re-entrant cavities provided the highest thermal performance, although at the cost of a higher pressure drop. Ghaedamini and colleagues[10] conducted a numerical investigation on the impact of geometric parameters on the hydrothermal performance in converging-diverging microchannels. Their analysis confirmed that increasing the wave amplitude generates turbulent flow, which enhances flow disturbance and, consequently, improves heat transfer.

Chai et al.[11] conducted a numerical analysis of laminar flow and heat transfer in a micro heat sink featuring obstacles on the walls. Their findings indicate that for Reynolds numbers less than 350, micro heat sinks with forward-facing triangular obstacles exhibit the highest performance. In contrast, heat sinks with rectangular obstacles demonstrate the weakest performance within this range. For Reynolds numbers greater than 400, semi-circular obstacles yield the best performance, while backward-facing triangular obstacles result in the poorest performance. The hydrothermal performance of a micro heat sink with bidirectional obstacles has been studied experimentally and numerically by Wang et al.[12]. They demonstrated that bidirectional obstacles enhance heat transfer by disrupting the thermal boundary layer and inducing rotation in both vertical and horizontal directions. As a result, the Nusselt number is maintained at a high level. Wang et al.[13] conducted a three-dimensional numerical simulation to investigate the hydrothermal performance of microchannels with cut-off obstacles arranged in parallel and stepped configurations. They observed that regions near the cut-off gaps exhibited higher Nusselt numbers due to the increased flow velocity. Additionally, the presence of cut-off gaps resulted in a reduced pressure drop, owing to the increased flow area.

Zheng et al.[14] conducted a numerical study on enhancing heat transfer in a channel with convergent and divergent slit ribs. It was found that high heat transfer performance between adjacent ribs could be achieved using these ribs. Wang et al.[15,16] experimentally and numerically investigated the heat transfer and friction characteristics of microfluidic heat sinks with variously shaped micro-ribs, including rectangular, triangular, and semicircular ribs. Their findings indicated that the use of micro-ribs enhanced the heat transfer rate; however, it also resulted in an increased pressure drop for the microchannels.

Vaferi et al. [17] conducted a numerical study on the impact of barrier geometry and heat sink substrate material on thermal resistance. Their findings indicate that replacing a silicon substrate with AlN ceramic reduces thermal resistance by approximately 31%, attributed to the ceramic's superior thermal conductivity. Additionally, they highlighted the significant influence of barrier geometry, demonstrating that a narrower barrier width leads to lower thermal resistance and enhances heat sink performance.

Wang et al. [18] explored two microchannel designs featuring symmetric and parallel wave walls with porous barriers. Their study revealed that fluid penetration into the porous ribs reduces the flow rate, leading to a decrease in pressure drop. Additionally, they found that the symmetric configuration further minimizes pressure drop, whereas the parallel arrangement enhances thermal performance.

Mirzaei et al. [19] conducted a numerical study on a 3D interrupted microchannel heat sink (MCHS) with diamond-shaped ribs to evaluate its thermal and hydraulic performance. Their findings confirmed that integrating ribs significantly enhances heat transfer compared to straight microchannels. Optimizing rib geometry further improves performance—reducing the rib aspect ratio and increasing rib size contribute to better heat transfer.

The study identified mid-height diamond-shaped ribs as the optimal configuration for maximizing heat transfer at equal pumping power. Additionally, microchannels with multiple ribs exhibited superior thermal performance, although variations between designs containing 2, 3, or 4 ribs were relatively small. Across a broad range of Reynolds numbers, the most efficient thermal enhancement was achieved with a rib aspect ratio of 1, a rib height of 120 µm, a rib number of 2, a rib scale exceeding 150 µm, and a microchamber length of 1300 µm.

Chai et al. [20] proposed the use of rectangular ribs in transverse microgrooves between discontinuous microchannels. Their experimental and numerical demonstrations showed that overall performance improved due to the higher enhancement of heat transfer compared to the pressure drop. No study has been done on the microchannel heat sink with multistep transverse ribs.

In this study, the heat transfer and flow characteristics of a microchannel heat sink with multistep transverse ribs were investigated numerically using ANSYS Fluent software. Double-step configurations have not been investigated before. Therefore, this study focused on the number of steps and the effect of the area ratio of each step to the lower step. To compare different configurations, the average Nusselt number and average friction factor along the microchannel were examined. The thermal enhancement factor of the microchannel was determined using the average Nusselt number and average friction factor.

2-Governing equations, boundary conditions, geometry and mesh

In the current study, the flow is considered steady, laminar, incompressible and a constant heat flux is applied to the bottom of the microchannel. Laminar flow is used in studies on microchannel heat exchangers because it aligns with their typical operating conditions, where low Reynolds numbers naturally result in laminar behavior. Studying laminar flow allows for accurate modeling of heat transfer characteristics and pressure drop, which are crucial for optimizing performance. Under the given assumptions, the governing equations for the conservation of mass, momentum, and energy related to convective heat transfer in microchannels can be articulated in the Cartesian tensor system as follows:

Continuity equation:

$$\frac{\partial}{\partial x_i}(\rho u_i) = 0 \tag{1}$$

Momentum equation:

$$\frac{\partial}{\partial x_i}(\rho_f u_i u_j) = -\frac{\partial P}{\partial x_j} + \frac{\partial}{\partial x_j}\left[\mu_f\left(\frac{\partial u_j}{\partial x_i} + \frac{\partial u_i}{\partial x_j}\right)\right] \tag{2}$$

Energy equation for the fluid domain is:

$$\frac{\partial}{\partial x_i}\left(\rho_f \vec{u_i} c_{\rho f} T\right) = \frac{\partial}{\partial x_i}\left(k_f \frac{dT}{dx_i}\right) + \mu_f\left[2\left(\frac{\partial \vec{u_i}}{\partial x_i}\right)^2 + \left(\frac{\partial \vec{u_j}}{\partial x_i} + \frac{\partial \vec{u_i}}{\partial x_j}\right)\right] \tag{3}$$

The energy equation for the solid domain is:

$$\frac{\partial}{\partial x_i}\left(k_s \frac{dT}{dx_i}\right) = 0 \tag{4}$$

In the present study, liquid water is used as the working fluid. The associated boundary conditions for the simulation are set as follows:
For microchannel inlet at x=0:

$$u = u_{in} \tag{5-A}$$
$$v = w = 0 \tag{5-B}$$
$$T_f = T_{in} = 293K \tag{5-C}$$

And for the solid surface at x=0:

$$\frac{\partial T_s}{\partial x} = 0 \tag{5-D}$$

At x=10mm, for microchannel outlet:

$$v = w = 0 \tag{6-A}$$
$$p_f = p_{out} = 1atm \tag{6-B}$$
$$\frac{\partial u}{\partial x} = \frac{\partial T_f}{\partial x} = 0 (for\ fluid) \tag{6-C}$$

For solid surface:

$$\frac{\partial T_s}{\partial x} = 0 \tag{6-D}$$

At walls (y=0 and y=0.25mm)

$$\frac{\partial T_s}{\partial y} = 0 \tag{7}$$

At the bottom of the channel (z=0):

$$q'' = q''_{in} \tag{8}$$

At the top of the channel (z=0.35mm):

$$u = v = w = 0 \tag{9-A}$$
$$\frac{\partial T_f}{\partial z} = \frac{\partial T_s}{\partial z} = 0 \tag{9-B}$$

At the inner walls:

$$u = v = w = 0 \tag{10-A}$$
$$-k_s\left(\frac{\partial T_s}{\partial n}\right) = -k_f\left(\frac{\partial T_f}{\partial n}\right) \tag{10-B}$$

where n is the local coordinate normal to the wall.
For the front and back of the microchannel, as well as the top surface, thermal insulation is applied. The symmetry condition is applied to the side walls. Additionally, an initial heat flux of 1.22 megawatts per square meter is applied to the bottom of the microchannel.
Reynolds number is defined as:

$$R = \frac{\rho u_m D_h}{\mu} \tag{11}$$

Where ρ is the fluid density, u_m is the mean inlet velocity of the fluid, D_h is the hydraulic diameter and μ is the fluid dynamic viscosity.
The average friction factor is defined as:

$$\bar{f} = \frac{2\ \Delta P\ D_h}{\rho\ L\ u_m{}^2} \tag{12}$$

with ΔP being the pressure drop across the length of the microchannel and L being the length of the microchannel. The pressure drop is calculated using the following expression:

$$\Delta P = \overline{P_{in}} - P_{out} \tag{13}$$

Where $\overline{P_{in}}$ is the mass-weighted average of the inlet pressure and P_{out} is the outlet pressure.
The average Nusselt number is evaluated based on the following expression:

$$\overline{Nu} = \frac{\bar{h} D_h}{k_f} \tag{14}$$

Where k_f represents the thermal conductivity of the fluid at the respective $\overline{T_f}$, with $\overline{T_f}$ being the mass-weighted average of the fluid temperature.
The average heat transfer coefficient is defined as:

$$\bar{h} = \frac{q''_{in} A_b}{A_{contact}\left(\overline{T_w} - \overline{T_f}\right)} \tag{15}$$

Where q'' represents the heat flux, A_b is the bottom heated wall area, $A_{contact}$ is the contact surface area between water and substrate for single microchannel, and $\overline{T_w}$ is the area-weighted average temperature of bottom heated wall.
The thermal enhancement factor is defined as the ratio of the average heat transfer coefficient of the interrupted microchannel ($\bar{h}$) to that of the rectangular straight microchannel ($\bar{h}_0$) [21] and is given by:

$$\eta = \frac{\overline{Nu}/\overline{Nu}_0}{(\bar{f}/\bar{f}_0)^{1/3}} \tag{15}$$

The dimensions of the designed micro heat sink are shown in Figure 1 and detailed dimensions of the rib are shown in Figure 2. To save simulation time, the simulation domain is limited to a single microchannel.
In this study, ANSYS Fluent was utilized to perform the simulation. To ensure grid independence, the velocity of the fluid at x=10mm along a vertical line from z=0.15 mm to z=0.35 mm was analyzed at the outlet. A mesh with 600000 elements was determined to be the optimal choice, as the change in velocity was minimal when the mesh size was increased to 800000 elements. The differences in velocity for various mesh sizes are illustrated in Figure 3.
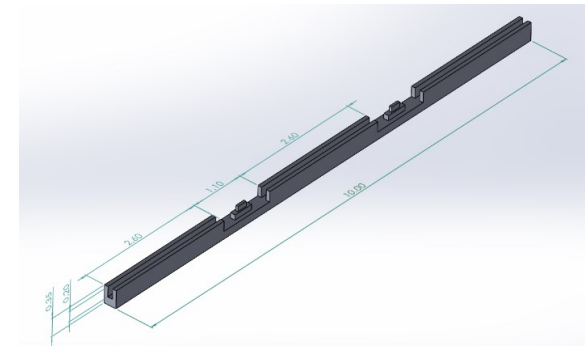
Figure 1 A single section of MCHS with double step ribs in transverse microchambers.
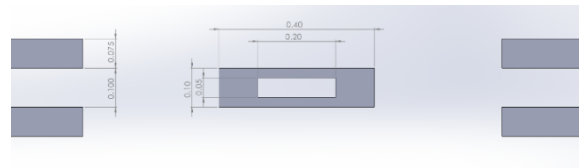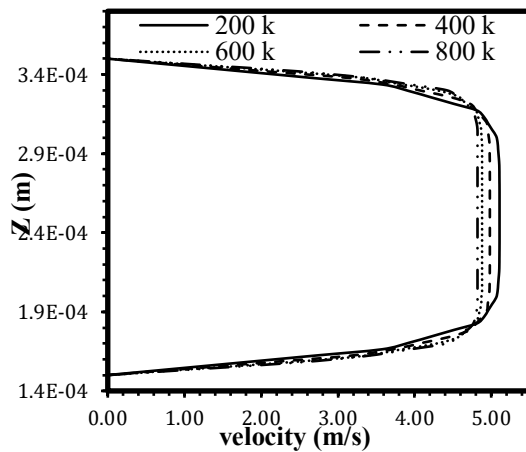

Figure 2 Detailed dimensions of the rib

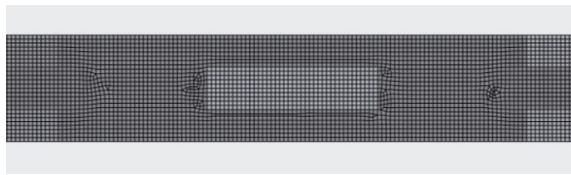**Figure 3** Velocity along a vertical line at the outlet

Figure 4 Chosen mesh elements from top view.

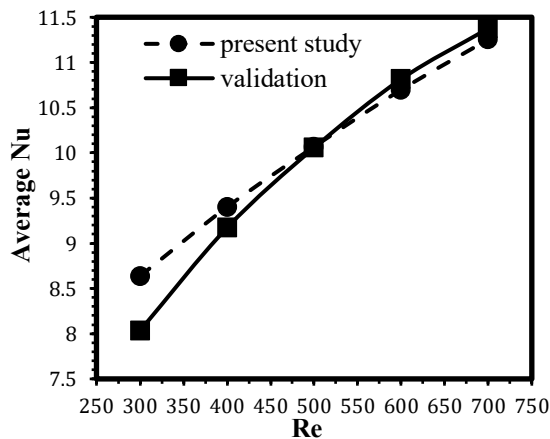Additionally, the selected mesh, viewed from the top, is shown in Figure 4.

Figure 5 validation of the present study with Chai et al. [17]

3-Validation

In order to validate the simulations in this study, the average Nusselt numbers for different Reynolds numbers in the microchannel were compared with the study carried out by Chai et al. [20], as shown in Figure 5. It is demonstrated that the present work has a maximum error of 6.98% compared to the previous study. Therefore, the present simulation is considered accurate.

4-Results and discussion

The results of $\overline{Nu}/\overline{Nu}_0$, $\overline{f}/\overline{f}_0$ and η for variable multi-step ribs with different step numbers are shown in Figure 6. In each step, the base area is half of the previous step. For the whole range of investigated Re, the values of $\overline{Nu}/\overline{Nu}_0$ and $\overline{f}/\overline{f}_0$ are more than unity meaning that microchannel with multi-step ribs has better heat transfer and more pressure drop than the microchannel with single-step ribs.

It is observed that double-step ribs exhibit better heat transfer enhancement compared to other step numbers, with the maximum improvement of the Nusselt number being 27.3% at a Reynolds number of 300. As the Reynolds number increases, this enhancement decreases. The second-best enhancement belongs to triple-step ribs, while the lowest enhancement is observed with four-step ribs. The

enhancement of the Nusselt number by adding steps to the rib is due to the vortices generated by the steps. However, adding more steps reduces the heat transfer surface area. Initially, the impact of the vortices is more significant than the reduction in surface area, up to the point of adding two steps. Beyond that, the reduction in surface area outweighs the impact of the vortices, resulting in decreased Nusselt number enhancement.

It is evident that the friction factor also increased due to the vortices generated. The friction factor is highest for double-step ribs, with a 41% increase at a Reynolds number of 500. In all cases, the friction factor initially increases and then begins to decrease after reaching Reynolds numbers around 500. This is because the vortices have a greater impact on increasing the friction factor at lower Reynolds numbers. However, as the Reynolds numbers increase, their effect becomes less dominant.

Taking into account both the Nusselt number and the friction factor in each case, the thermal enhancement factor is introduced to show the simultaneous effects of Nusselt number and friction factor. While a higher Nusselt number indicates better heat transfer, it is also associated with an increase in the friction factor. An increased friction factor results in higher energy costs due to increased pressure drops and may necessitate costly system upgrades, driving up operational expenses. Therefore, a balance between improved heat transfer and the increase in friction factor is essential. The thermal enhancement factor is highest for the double-step ribs and lowest for the four-step ribs, with increases of 14% and 7%, respectively, at a Reynolds number of 300. This suggests that double-step ribs offer superior heat transfer performance while minimizing the additional energy required for pumping. Consequently, the use of double-step ribs is considered optimal, as they provide efficient heat transfer without excessively increasing energy consumption.
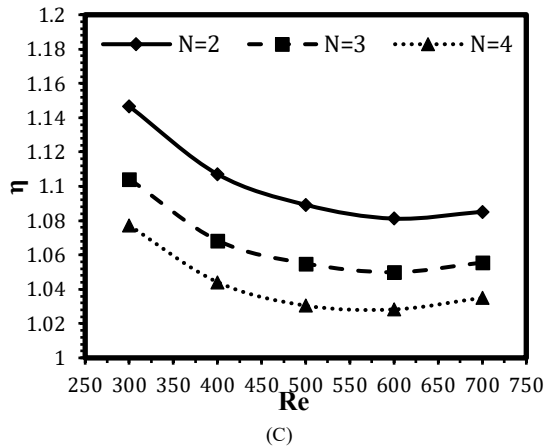

(A)

(B)

(C)
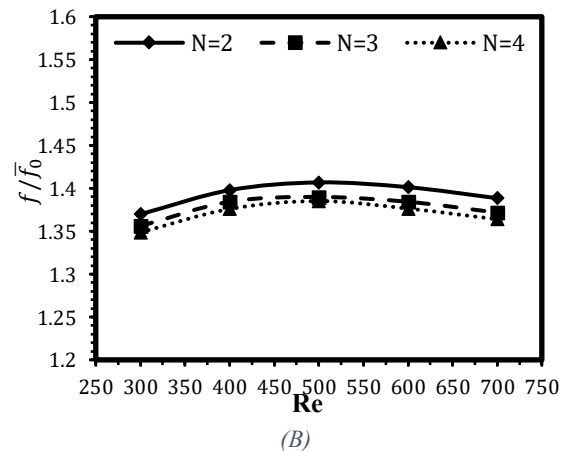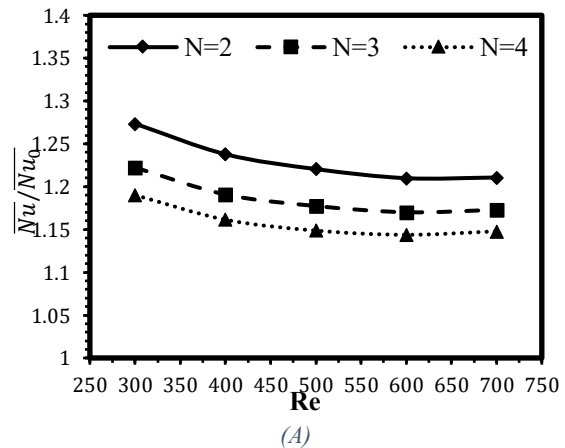
Figure 6 (A) Variation of $\overline{Nu}/\overline{Nu}_0$, (B) variation of $\overline{f}/\overline{f}_0$ and (C) variation of η with Re for different multi-step ribs

Table 1 Variation of $\overline{Nu}/\overline{Nu}_0$ with Re for different multi-step ribs

Steps/Re	300	400	500	600	700
2	1.27	1.24	1.22	1.21	**1.21**
3	1.22	1.19	1.18	1.17	**1.17**
4	**1.19**	**1.16**	**1.15**	**1.14**	**1.14**

Table 2 Variation of $\overline{f}/\overline{f}_0$ with Re for different multi-step ribs

Steps/Re	300	400	500	600	700
2	1.37	1.4	1.41	1.4	**1.39**
3	1.36	1.38	1.39	1.38	**1.37**
4	**1.35**	**1.37**	**1.38**	**1.37**	**1.36**

The effects of Reynolds numbers on $\overline{Nu}/\overline{Nu}_0$ and $\overline{f}/\overline{f}_0$ across different step numbers are summarized in Table 1 and Table 2, respectively.

As concluded in the previous section, double-step ribs demonstrate the highest efficiency. The results of $\overline{Nu}/\overline{Nu}_0$, $\overline{f}/\overline{f}_0$ and η for double-step ribs with different base surface areas are shown in Figure 7. Four configurations are studied, with varying base surface areas for the top step, denoted as A_2. The heights of both the top and lower steps are equal in all configurations. It is observed that the highest Nusselt number value, and consequently the best heat transfer, occurs in the configuration where A_2=1.5A resulting in a 42% increase at a Reynolds number of 300. A significant disparity is noted between increasing and decreasing the top step base surface area.

It can be concluded that larger surface areas result in greater heat transfer. However, attention must be paid to the friction factor, which also increases with an increase in surface area. The highest friction factors are observed in the configuration with A_2=1.5A, showing a 51% increase at a Reynolds number of 500. The behavior of the friction factors follows a similar pattern as discussed previously, with an initial increase followed by a decrease due to the dominance of velocity over the vortices generated by the steps.

The thermal enhancement factor has the highest value for the configuration A_2=1.5A, reaching a maximum of 25% at a Reynolds number of 300. However, it decreases as the Reynolds number increases.

The effects of Reynolds numbers on $\overline{Nu}/\overline{Nu}_0$ and $\overline{f}/\overline{f}_0$ across different areas of two-step ribs are summarized in Table 3 and Table 4, respectively.
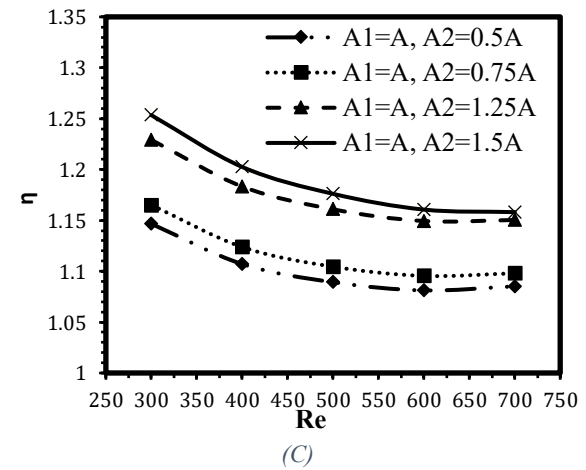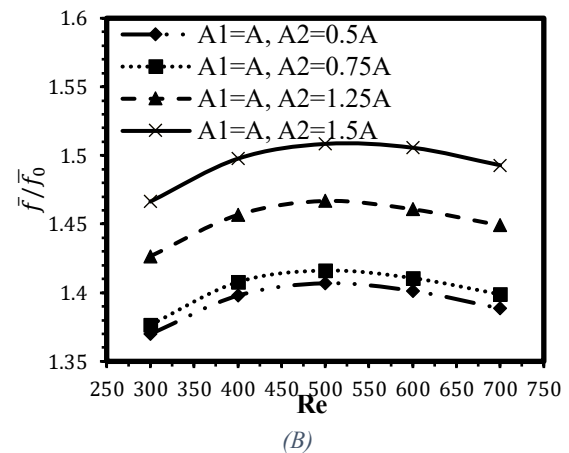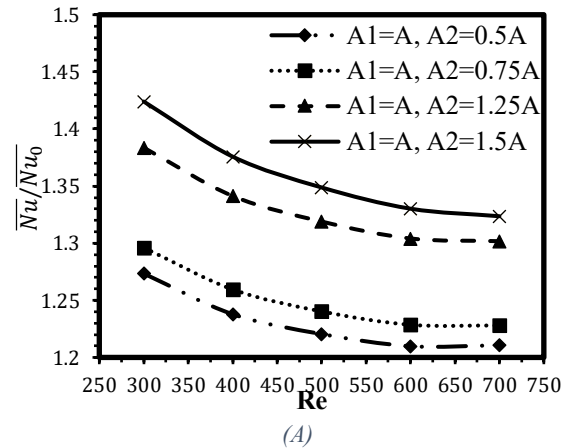

(A)

(B)

(C)

Figure 7 (a) Variation of $\overline{Nu}/\overline{Nu}_0$, (b) variation of $\overline{f}/\overline{f}_0$ and (c) variation of η with Re for different areas of two-step ribs

Table 3 Variation of $\overline{Nu}/\overline{Nu}_0$ with Re for different areas of two-step ribs, using the base rib area A

A2/Re	300	400	500	600	700
0.5A	1.27	1.24	1.22	1.21	**1.21**
0.75A	1.3	1.26	1.24	1.23	**1.23**
1.25A	1.38	1.34	1.31	1.3	**1.3**
1.5A	**1.42**	**1.38**	**1.35**	**1.33**	**1.32**

Table 4 Variation of $\overline{f}/\overline{f}_0$ with Re for different areas of two-step ribs, using the base rib area A

A2/Re	300	400	500	600	700
0.5A	1.37	1.4	1.41	1.4	1.39
0.75A	1.38	1.41	1.42	1.41	1.4
1.25A	1.43	1.46	1.47	1.46	1.45
1.5A	1.47	1.5	1.51	1.51	1.49

Nomenclature

A_b	Bottom heated wall area, m^2
$A_{contact}$	Contact surface area of water and silicon for single microchannel, m^2
A	Base surface area of ribs, m^2
A_2	Surface area of the top rib in a double-step rib, m^2
D_h	Hydraulic diameter, m
$\overline{f}$	Average friction factor
$\overline{h}$	Average heat transfer coefficient, Wm^{-2}K^{-1}
k	Thermal conductivity, Wm^{-1}K^{-1}
L	Overall length of the MCHS, m
n	Local coordinate normal to the wall
P	Static pressure, Pa
q	Heat applied, W
q''	Heat flux at the back surface of the silicon substrate, W.m^{-2}
T	Temperature, K
T_w	Bottom heated wall temperature, K
T_f	Fluid temperature, K
u_m	Mean velocity, m.s^{-1}
ρ	Density, kgm^{-3}
μ	Dynamic viscosity, Pa S
η	Thermal enhancement factor

Conclusions

In previous studies, single-step ribs were investigated; however, this study focuses on the performance of multi-step ribs in microchannel heat sinks. The aim was to understand how the number of steps and the base surface area of the ribs impact heat transfer and friction factor. Various configurations were analyzed, including single, double, triple, and four-step ribs, with a focus on optimizing the thermal enhancement factor. The results indicated that double-step ribs offered the best performance among the configurations studied, providing the most efficient balance between improved heat transfer (27%) and increased friction factor (41%), with the thermal enhancement factor increased by 14%. Additionally, different surface areas for the top step of a double-step rib were investigated, and it was found that the configuration with A_2=1.5A was the most effective, with a 25% increase in the thermal enhancement factor due to its higher heat transfer surface area. These findings highlight the potential of double-step rectangular ribs with larger top step surface areas as the most effective design for practical applications in thermal management systems. Other ribs with different shapes can be considered for investigation in future studies.

Ethics Approval

The scientific content of this article is the result of the authors' research and has not been published in any Iranian or international journal.

Conflict of Interest

This article includes some results from the corresponding author's doctoral dissertation. There are no other conflicts of interest to declare

References

[1] M. Dogan and M. Sivrioglu, "Experimental investigation of mixed convection heat transfer from longitudinal fins in a horizontal rectangular channel," *Int. J. Heat Mass Transfer*, vol. 53, no. 7-8, pp. 2149–2158, May 2010. . DOI: 10.48311/mme.24.11.9.
[2] Y. Sui, P. S. Lee, and C. J. Teo, "An experimental study of flow friction and heat transfer in wavy microchannels with rectangular cross section," *Int. J.*

Thermal Sci., vol. 50, no. 11, pp. 2473–2482, Nov. 2011.DOI: 20.1001.1.10275940.1393.14.10.1.6.
[3] N. R. Kuppusamy, H. A. Mohammed, and C. W. Lim, "Numerical investigation of trapezoidal grooved microchannel heat sink using nanofluids," *Thermochim. Acta*, vol. 573, pp. 39–56, 2013. DOI: 10.1016/j.ijheatmasstransfer.2009.12.031.
[4] N. R. Kuppusamy, H. A. Mohammed, and C. W. Lim, "Thermal and hydraulic characteristics of nanofluid in a triangular grooved microchannel heat sink (TGMCHS)," *Appl. Math. Comput.*, vol. 246, pp. 168–183, 2014. DOI: 10.1016/j.ijthermalsci.2011.06.017.
[5] G. Xia, L. Chai, M. Zhou, and H. Wang, "Effects of structural parameters on fluid flow and heat transfer in a microchannel with aligned fan-shaped reentrant cavities," *Int. J. Thermal Sci.*, vol. 50, pp. 411–419, May 2011. DOI: 10.1016/j.tca.2013.07.023.
[6] L. Chai, G. Xia, M. Zhou, and J. Li, "Numerical simulation of fluid flow and heat transfer in a microchannel heat sink with offset fan-shaped reentrant cavities in sidewall," *Int. Commun. Heat Mass Transfer*, vol. 38, pp. 577–584, 2011. DOI: 10.1016/j.amc.2014.07.087.
[7] G. Xia, L. Chai, H. Wang, M. Zhou, and Z. Cui, "Optimum thermal design of microchannel heat sink with triangular reentrant cavities," *Appl. Thermal Eng.*, vol. 31, pp. 1208–1219, 2011. DOI: 10.1016/j.ijthermalsci.2010.10.015.
[8] L. Chai, G. Xia, L. Wang, M. Zhou, and Z. Cui, "Heat transfer enhancement in microchannel heat sinks with periodic expansion–constriction cross-sections," *Int. J. Heat Mass Transfer*, vol. 62, pp. 741–751, 2013. DOI: 10.1016/j.icheatmasstransfer.2010.12.037.
[9] G. D. Xia, J. Jiang, J. Wang, Y. L. Zhai, and D. D. Ma, "Effects of different geometric structures on fluid flow and heat transfer performance in microchannel heat sinks," *Int. J. Heat Mass Transfer*, vol. 80, pp. 439–447, 2015. DOI: 10.1016/j.applthermaleng.2010.12.022.
[10] H. Ghaedamini, P. S. Lee, and C. J. Teo, "Developing forced convection in converging–diverging microchannels," *Int. J. Heat Mass Transfer*, vol. 65, pp. 491–499, May 2013. DOI: 10.1016/j.ijheatmasstransfer.2013.02.013.
[11] L. Chai, G. D. Xia, and H. S. Wang, "Numerical study of laminar flow and heat transfer in microchannel heat sink with offset ribs on sidewalls," *Appl. Thermal Eng.*, vol. 92, pp. 32–41, 2016. DOI: 10.1016/j.ijheatmasstransfer.2014.09.017.
[12] G. Wang, N. Qian, and G. Ding, "Heat transfer enhancement in microchannel heat sink with bidirectional rib," *Int. J. Heat Mass Transfer*, vol. 136, pp. 597–609, 2019. DOI: 10.1016/j.ijheatmasstransfer.2013.06.036.
[13] G. Wang, T. Chen, M. Tian, and G. Ding, "Fluid and heat transfer characteristics of microchannel heat sink with truncated rib on sidewall," *Int. J. Heat Mass Transfer*, vol. 148, p. 119142, 2020. DOI: 10.1016/j.applthermaleng.2015.09.071.
[14] D. Zheng, X. Wang, and Q. Yuan, "The flow and heat transfer characteristics in a rectangular channel with convergent and divergent slit ribs," *Int. J. Heat Mass Transfer*, vol. 141, pp. 464–475, 2019. DOI: 10.1016/j.ijheatmasstransfer.2019.05.115.
[15] G. L. Wang, D. W. Yang, Y. Wang, D. Niu, X. L. Zhao, and G. F. Ding, "Heat transfer and friction

characteristics of the microfluidic heat sink with variously-shaped ribs for chip cooling," *Sensors (Basel)*, vol. 15, no. 4, pp. 9547–9562, 2015. DOI: 10.1016/j.ijheatmasstransfer.2019.119142.

[16] J. Luo, G. Wang, Y. Sun, X. Zhao, and G. Ding, "Microengineering, fabrication and characterization of a low-cost interposer with an intact insulation layer and ultra-low TSV leakage current," *J. Micromech. Microeng.*, vol. 28, no. 12, p. 125010, 2018. DOI: 10.1016/j.ijheatmasstransfer.2019.06.060.

[17] K.Vaferi, M.Vajdi, S.Nekahi, S.Nekahi, F.S.Moghanlou, S.Azizi, and M.S.Asl, "Numerical simulation of cooling performance in microchannel heat sinks made of AlN ceramics," *Microsyst.Technol.*, vol.29, no.1, pp.141–156, 2023. DOI: 10.1007/s00542-022-05400-x. DOI: 10.3390/s150409547.

[18] S.-L. Wang, D. An, Y.-R. Yang, S.-F. Zheng, X.-D. Wang, and D.-J. Lee, "Heat transfer and flow characteristics in symmetric and parallel wavy microchannel heat sinks with porous ribs," *Int. J. Therm. Sci.*, vol. 185, p. 108080, 2023. DOI: 10.1088/1361-6439/aae8da.

[19] A.M. Mirzaei, A. Ramiar, and R. Derakhshan, "Numerical investigation of an interrupted microchannel heat sink with diamond-shaped ribs in transverse microchambers," *J.Therm.Anal.Calorim.*, vol.185, p.108080, 2024. DOI: 10.1007/s00542-022-05400-x.

[20] L. Chai, G. Xia, M. Zhou, J. Li, and J. Qi, "Optimum thermal design of interrupted microchannel heat sink with rectangular ribs in the transverse microchambers," *Appl. Thermal Eng.*, vol. 51, pp. 880–889, 2013. DOI: 10.1016/j.ijthermalsci.2022.108080.

[21] R. Karwa, C. Sharma, and N. Karwa, "Performance evaluation criterion at equal pumping power for enhanced performance heat transfer surfaces," *J. Solar Energy*, vol. 2013, pp. 1–9, 2013. DOI: 10.1007/s10973-024-13856-4.